Near-Eye Varifocal Augmented Reality Display using See-Through Screens

KAAN AKŞIT, NVIDIA Corporation
WARD LOPES, NVIDIA Corporation
JONGHYUN KIM, NVIDIA Corporation
PETER SHIRLEY, NVIDIA Corporation
DAVID LUEBKE, NVIDIA Corporation

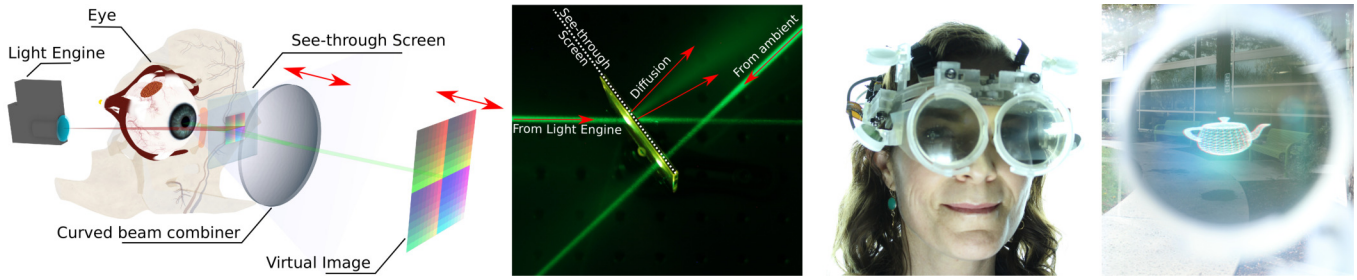

Fig. 1. Our proposal for a see-through, varifocal, near-eye display. Left: A light engine projects an image onto a thin, light-weight, see-through screen directly in front of the eye. The resulting image is relayed to a desired optical depth determined by the distance from the screen to the curved beam combiner. Middle left: Importantly, the screen is a hologram designed so that laser beams coming from each side act differently – light from the light engine diffuses towards the beam combiner while external light from the environment (and reflected light from the beam combiner) pass through the screen. Middle right: A wearable prototype uses two light engines through two optical folds to project onto the screens. Right: A daylight photo taken from the eye position demonstrates the brightness achieved by our design.

We present a new optical design for see-through near-eye displays that is simple, compact, varifocal, and provides a wide field of view with clear peripheral vision and large eyebox. Key to this effort is a novel see-through rear-projection screen. We project an image to the see-through screen using an off-axis path, which is then relayed to the user's eyes through an on-axis partially-reflective magnifying surface. Converting the off-axis path to a compact on-axis imaging path simplifies the optical design. We establish fundamental trade-offs between the quantitative parameters of resolution, field of view, and the form-factor of our design. We demonstrate a wearable binocular near-eye display using off-the-shelf projection displays, custom-designed see-through spherical concave mirrors, and see-through screen designs using either custom holographic optical elements or polarization-selective diffusers.

CCS Concepts: • **Human-centered computing → Displays and imagers**; • **Applied computing → Physics**; • **Hardware → Emerging optical and photonic technologies**;

Additional Key Words and Phrases: Near eye displays, See-through Displays, Varifocal Displays, Computational Displays, Augmented Reality Displays, Holography, Holographic Optical elements

0730-0301/2017/11-ART1 $15.00
https://doi.org/10.1145/3130800.3130892

ACM Reference format:
Kaan Akşit, Ward Lopes, Jonghyun Kim, Peter Shirley, and David Luebke. 2017. Near-Eye Varifocal Augmented Reality Display using See-Through Screens. *ACM Trans. Graph.* 36, 6, Article 1 (November 2017), 13 pages.
https://doi.org/10.1145/3130800.3130892

1 INTRODUCTION

Augmented reality (AR) has recently gained momentum in the form of a variety of available optical see-through near-eye displays (NEDs) including the Meta 2, the Sony Smart Eye, and the Microsoft Hololens. Kress and Sterner [2013] described the goal of consumer-level AR NEDs as providing a cost-effective solution to multiple optical design challenges: resolution, transparency, eyebox, and field of view (FoV). Cakmakci et al. [2006] point out FoV as the major optical design challenge. There is also increasing evidence that accommodation-aware systems improve user experience in Virtual Reality (VR) and AR systems [Konrad et al. 2016; Kramida and Amitabh 2016; Liu et al. 2008]. Addressing all of these characteristics is an ongoing challenge in AR NED design. We present a new configuration for an AR NED that provides the following contributions:

- *See-through screens for near-eye displays:* We introduce *on-axis see-through intermediate image surface* (OASIIS) screens, which address a major problem in optical AR NED design by providing an on-axis path for optical combiners, while avoiding significant perceptual degradation of the real world.

Table 1. Comparison of recent accommodation supporting see-through near eye displays (modeled after tables in Dunn et al. [2017] and Matsuda et al. [2017]). Our prototype demonstrates a unique combination of good from factor, resolution, FoV, and eyebox. Note that, in our chart, wide field of view is defined as $\geq 60^o$ degrees, high resolution is defined as ≥ 15 cycles per degree (cpd), and a moderate eyebox is defined as $5 - 10$ mm.

	Focus mechanism	FoV	resolution	eyebox	form factor	compute overhead
Pinlight displays [Maimone et al. 2014]	always in focus	wide	low	moderate	thin	high
Free-form optics [Hua and Javidi 2014]	light fields	narrow	high	moderate	moderate	high
HOE [Kim et al. 2015]	holographic	wide	high	small	bulky	N/A
HOE [Maimone et al. 2017]	holographic	wide	high	small	N/A	high
Focus tunable light engine [Liu et al. 2008]	varifocal	narrow	high	small	bulky	moderate
Multi-focal plane display [Hu and Hua 2014]	varifocal	narrow	high	moderate	bulky	high
Membrane [Dunn et al. 2017]	varifocal	wide	high	large	bulky	low
This work	varifocal	wide	high	large	moderate	low

- *Wide FoV:* The use of on-axis beam combiners with a large aperture size leads to a wide FoV.
- *Large eyebox:* The combination of traditional beam combiners and the novel see through screen leads to a large eyebox.
- *Simple varifocal mechanism:* The focal plane can be adjusted by mechanically moving thin and light optical components.
- *Wearable prototype:* As a proof of concept, we make and test a wearable AR NED. Our prototype employs two off-the-shelf projectors, two concave see-through mirrors, a mechanical linear actuator, and two OASIIS screens in a 3D printed housing. The prototype provides brightness levels suitable for indoor and outdoor applications.

We believe this design lends itself to straightforward miniaturization. Each component is relatively cheap to manufacture and the design will benefit from continuing improvements of picoprojectors and actuators. Critically, the design can support an accommodation-aware system, by integrating a (commercially available) gaze tracker and a fast linear mechanism for moving the optical components; we also demonstrate this capability with our prototype. The least straightforward element of our design is the OASIIS screen, which we describe in detail in this paper.

2 RELATED WORK

Our design is a see-through AR NED with a simple varifocal mechanism aimed at future accommodation-aware systems. We here review see-through AR screens used in non-NED contexts, other NED AR optics designs, and finally accommodation-aware NED designs in both AR and VR contexts. We do not review direct retinal projection AR systems [Urey 2000] nor video see-through AR systems [Rolland and Fuchs 2000] which are completely different approaches to AR than the beam-splitter family of designs to which ours belongs. These different families of approaches have different advantages and disadvantages and all three are being actively pursued by the AR community. Our prototype is contrasted with other optical see-through AR NEDs in Table 1. These are all research prototypes so the table does not show what the limits are in the various approaches, but they do indicate how far the various approaches can definitely be pushed.

2.1 See-through Screens:

Researchers have explored see-through screen designs based on classical optical components. Hedili et al. [2013] describe a see-through microlens array for a heads-up display application. Soomro and Urey [2016] report a see-through screen based on retro-reflectors for a head mounted projection display application. Neither of these approaches has yet been redesigned for NEDs, nor for the expected diffraction effects accompanying that miniaturization.

Using silver nanoparticles and a front projector, Hsu et al. [2014] create a transparent screen that backscatters light at specific wavelengths. Yamamoto et al. [2016] also describe a different approach to a wavelength selective front projection transparent screen using *cholesteric liquid crystal dots*. Both approaches scatter light in both the forward and reverse directions which can lead to a strong perceivable haze in a NED application.

Holographic optical elements (HOEs) are able to direct light from a carefully placed light source towards a user's eye while appearing transparent to light from the environment. HOEs have been used as optical components in transparent heads-up displays [Tolstik et al. 2009]. Lee et al. [2016] used two reflective diffusive HOEs and two projectors to create a transparent additive light field display that is in a similar spirit to our OASIIS screen, but is front-projection and not for NED. Reflective and diffusive holographic combiners have been used for transparent screens [Eisen et al. 2006; Yeom et al. 2014]. HOEs can also be used to redirect light from an off-axis projector into the eye [Kim et al. 2015; Maimone et al. 2017]. This serves the same function as our HOE and beam combiner together and has great potential for compactness and transparency but so far has unresolved issues with eyebox, and demands more compute before projection than our approach.

Spatial light modulators (SLMs), such as OLEDs or LCDs, can also function as see-through screens. Görrn et al. [2006] introduced entirely transparent displays using OLEDs with transparent contacts and thin-film transistors.

However, the periodic aperture arrangement in SLMs can cause diffraction-related image degradation over the observed real world; Using LCDs directly in front of an eye, Maimone et al. [2014] shows a typical example of such degradation. LCDs with polarizers also block certain polarizations of the light. Tsai et al. [2015] propose a custom aperture arrangement for avoiding degradation with OLEDs which is similar to coded-aperture techniques [Ma et al. 2013]. Thus,

it improves some details of the real world while degrading others. Since we do not use SLMs as see-through screens, we avoid these shortcomings.

2.2 See-through NED Optics:

Sutherland [1968] introduced see-through NEDs using a beam combiner near the eye of a subject to superimpose the direct view of the real world and computer-generated images. Optical systems relying on flat combiners have progressed greatly as described by Rotier [1989] and Cakmakci, [Cakmakci and Rolland 2006]. The geometry of flat beam combiners along with the lenses used in optical NEDs dictates a strict trade-off: a large FoV quickly leads to a bulky form factor. Droessler et al. [1990] propose a tilted catadioptric (reflecting and refracting) system to overcome FoV limitations by tilting the optics with respect to a flat combiner and using a curved combiner as the final relay surface, which provides up to 60^o of rotationally symmetrical monocular FoV. Tilted catadioptric systems are fundamentally limited in light efficiency, depend on a complex polarized optical system, and produce a bulky form factor. Gilboa [1991] propose an off-axis single-element curved beam combiner, and explore the associated optical design space. Today, modern variants of off-axis single-element curved beam combiners (e.g., [Wang et al. 2016]) are deployed in military applications and consumer level prototypes (e.g., Meta 2). Major limitations in off-axis single-element curved beam combiners come into play while extending FoV in horizontal directions when lit vertically; these combiners are known to provide poor imaging characteristics with eccentricity, and require a larger screen with a larger FoV demand. Our optical layout builds on concepts shared with these systems. We essentially convert off-axis projection paths to on-axis paths using our OASIIS screens, which avoids the shortcomings of previous optical designs and provides a compact optical layout.

Another family of see-through NEDs is based on waveguides. Cheng et al. [2009] propose a waveguide based NED design that fuses curved beam combiners and waveguides into a single free-form prism. They describe a tiling strategy of these prisms to increase limited-FoV, which requires multiple displays per prism. Flat combiners have been converted into thin cascaded waveguides as a see-through NED prototype (e.g., Lumus), however FoV related issues are still a major problem in practice. As described by Kress and Shin [2013], holographic methods simplify designing waveguides through holographic out-coupling and in-coupling of light. Today such displays are present as consumer level see-through NED prototypes (e.g., Microsoft Hololens, Sony Smart Eye), which only report maximum 45^o diagonal binocular FoV. HOEs can function as a complete reflective and diffusive beam combiner (e.g., Li et al. [2016], Maimone et al. [2017]) with a small eyebox. Specifically, the work of Maimone et al. [2017] promises a glasses form factor see-through NED design, the chief limitations relative to our design are as follows: device runs 20 Hz refresh rate for generating full-color images, provides an impractical small eyebox, and demands a large computation. We demonstrate a practical use case of HOEs with our optical layout. The true potentials of HOEs in practical NED designs are yet to be explored.

Notably, most of these optical layouts block a large portion of peripheral vision, whereas our design leaves peripheral vision clear.

2.3 Accommodation Supporting See-through NEDs:

A major problem with NEDs is the *vergence-accommodation conflict* (VAC), where the binocular triangulation distance conflicts with the focusing distance [Shibata et al. 2005]. Early on, Akeley et al. [2004] demonstrate benefits of fixed-viewpoint volumetric desktop displays using planar multi planes and generate near-correct focus cues without tracking eye position. Using the hardware layout of work of Akeley et al. [2004], Mackenzie et al. [2010] describe the link between displayed spatial frequencies and human eye accommodation has a correlation. Work of Hu et al. [2014] demonstrate that planar multiple planes can also be used to discretize the planes of focus in a see-through NED design. Most recently, work of Matsuda et al. [2017] introduce a new concept for NED design for VR using the concept of deformed focus planes, and work of Konrad et al. [2017] propose an accommodation-invariant NED VR design. Kramida and Varshney [2016] , Masia et al. [2013] and Hong Hua [2017] give a recent and comprehensive review of different computational NED approaches to resolve VAC. Studies show evidence that supporting accommodative cues through a varifocal mechanism improves visual comfort [Johnson et al. 2016] and user performance [Konrad et al. 2016] while being simpler than other methods, but most current approaches sacrifice FoV and bulk. The recent design of Dunn et al. [2017] provides a wide FoV and a fast varifocal mechanism, but the flexible membrane mirror used as the outer optical surface presents cosmetic and physical robustness difficulties for long-term usage.

Integral Imaging, first proposed by Lippmann [1908], deals with the capture and the reproduction of lightfields which can also address VAC. Huang et al. [2015] demonstrate a factorized compressive lightfield for conventional NED VR design. A see-through NED design [Hua and Javidi 2014] uses a free-form prism from the work of Cheng et al. [2009], while supporting lightfields in a limited FoV. The work of Maimone et al. [2014] promises a wide FoV with see-through capabilities, but diffraction effects limit image quality; liquid-crystal switching times also limit their demonstrated prototype to 12 Hz refresh rate for full-color images. HOEs have been demonstrated in the context of generating lightfield displays [Lee et al. 2016], though not applied to NEDs, yet.

Similar to the mechanism we use to adjust focus, some systems have dynamically adjusted the distance between lens and screen [Liu et al. 2008; Padmanaban et al. 2017; Sugihara and Miyasato 1998]. Inspired by previous work, we propose a see-through NED design with a novel application of HOEs as OASIIS screens, opening the door to accommodation support while providing high refresh rate, full-color, improved resolution, wide FoV, large eyebox, and low compute overhead.

3 SYSTEM OVERVIEW

The overall structure of an optical see-through NED can be summarized as two separate building blocks: a light engine and a beam combiner. As shown in Figure 2, we place an OASIIS screen in front of a viewer's eye to relay information from an off-axis rear-projection light engine to an on-axis beam combiner. This on-axis component decreases the design complexity of the beam combiner,

and avoids fundamental limitations in both image quality and FoV without substantially blocking peripheral vision.

The OASIIS screen acts as an intermediate image plane. Optical NED designs with intermediate image planes are commonly known as pupil-forming optical layouts [Cakmakci and Rolland 2006]. In our design, the required size of a projected image d_{scr} depends on the nature of the curved beam combiner. Thus, we first explore the design space of curved beam combiners.

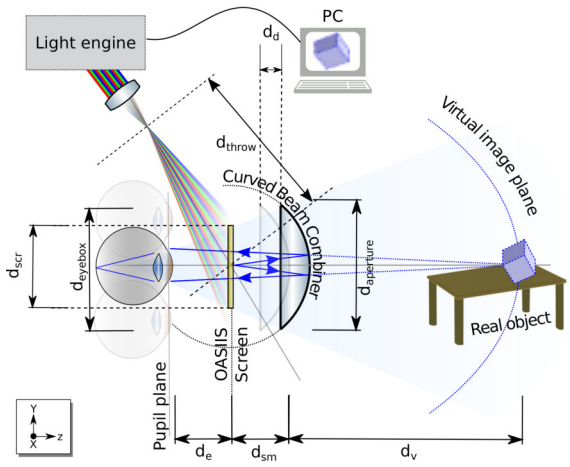

Fig. 2. The optical layout of our see-through Near-Eye Display proposal: An off-axis light engine projects information on an OASIIS screen. Projected information on the OASIIS screen is relayed back to a viewer's eye, while being magnified and placed at a virtual image plane by a curved beam combiner.

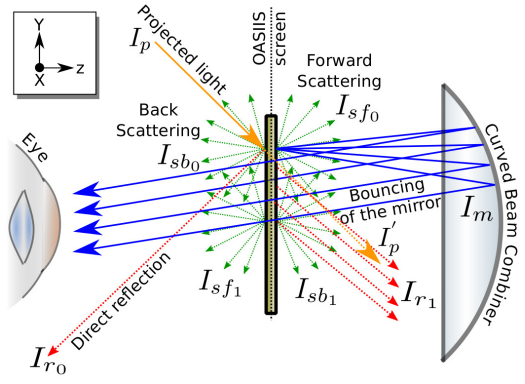

Fig. 3. A sketch showing major components of light rays that are interacting with an OASIIS screen that is located between an eye and a curved beam combiner. Stronger combiner reflectivity I_m and screen forward scattering I_{sf_o} lead to better image quality.

3.1 Curved Beam Combiners:

A curved optical beam combiner can be designed with specific demands in mind, such as, FoV, angular resolution, and size of *eyebox*, d_{eyebox}, the volume within which the pupil can move (Figure 2). The human visual system (HVS) spans approximately 190^o FoV horizontally [Webb 1964] and, with healthy young eyes (20/20 vision), approximately 1 arc-minute of angular resolution or 30 cycles per degree (cpd). We target d_{eyebox} of 10×10 mm to accommodate gaze changes without degrading optical quality. We use $d_e = 20$ mm, distance between the eye and the OASIIS screen, which leaves enough free-space propagation volume for our projection-based light engine.

Figure 3 shows a ray tracing diagram for an OASIIS screen. Light rays originated from a projector I_p will introduce multiple components as light reflects I_{r_0}, I_{r_1}, and scatters in forward I_{sf_0}, I_{sf_1} and back I_{sb_0}, I_{sb_1} directions. The major component of light contributing to the formation of a target image on a retina is the light that is bouncing from a curved beam combiner I_m and making its way to the retina. Note that I_m becomes a stronger component as I_{sf_0} dominates the scattering terms. For explanatory purposes, consider an ideal flat rectangular OASIIS screen. Such a screen provides forward diffusion I_{sf_0} as the major component, thus leading to a strong I_m while other components of light are negligibly small.

A simple solution is to use a spherical beam combiner with a radius of curvature r, and thus a focal length $f = -r/2$. The center of an OASIIS screen can be registered to a virtual point in space located at a desired distance d_v from a spherical beam combiner by using

$$\frac{1}{d_v} = \frac{1}{f} + \frac{1}{d_{sm}} \quad \Leftrightarrow \quad d_v = \frac{1}{\frac{1}{f} + \frac{1}{d_{sm}}} \tag{1}$$

where d_{sm} represents the distance between the mirror and the screen. Magnification of the screen can be calculated as $M = h_v/h_s = -d_v/d_{sm}$, where h_v represents the size of a virtual image created, and h_s represents the size of the screen. Total optical path length of our proposal using an OASIIS screen and a spherical beam combiner is expressed as $OPL = d_{sm} + d_e$. Using the provided equations and an in-house ray tracer, we compile a design trade space for our proposal, showing the optical qualities of designed beam combiners with required physical dimensions (Figure 4). We limit our spherical beam combiner to a f-number of $f/0.6$ to avoid large image degradations with increasing eccentricities. This sample choice represents a simpler design process compared to using other conic or freeform surfaces, each with multiple variables to tune.

3.2 OASIIS Screens:

The most important component of our design is an OASIIS screen. We evaluated multiple approaches: rotating diffusers, *polarization selective diffusers* (PSDs), and, most successfully, HOEs. We explain the theory and construction of HOEs here. We include details which will be known to those with a practical holography background but may not be familiar to others. For the interested reader, multiple, accessible and detailed introductions to holography and making HOEs exist, see for instance, Saxby and Zacharovas [2016] or Ackerman and Eichler [2007].

The interference from two coherent light beams, traditionally called reference and object beams, creates a diffraction pattern which can be recorded in a holographic recording medium (HRM). When the holographic diffraction pattern has been properly exposed and

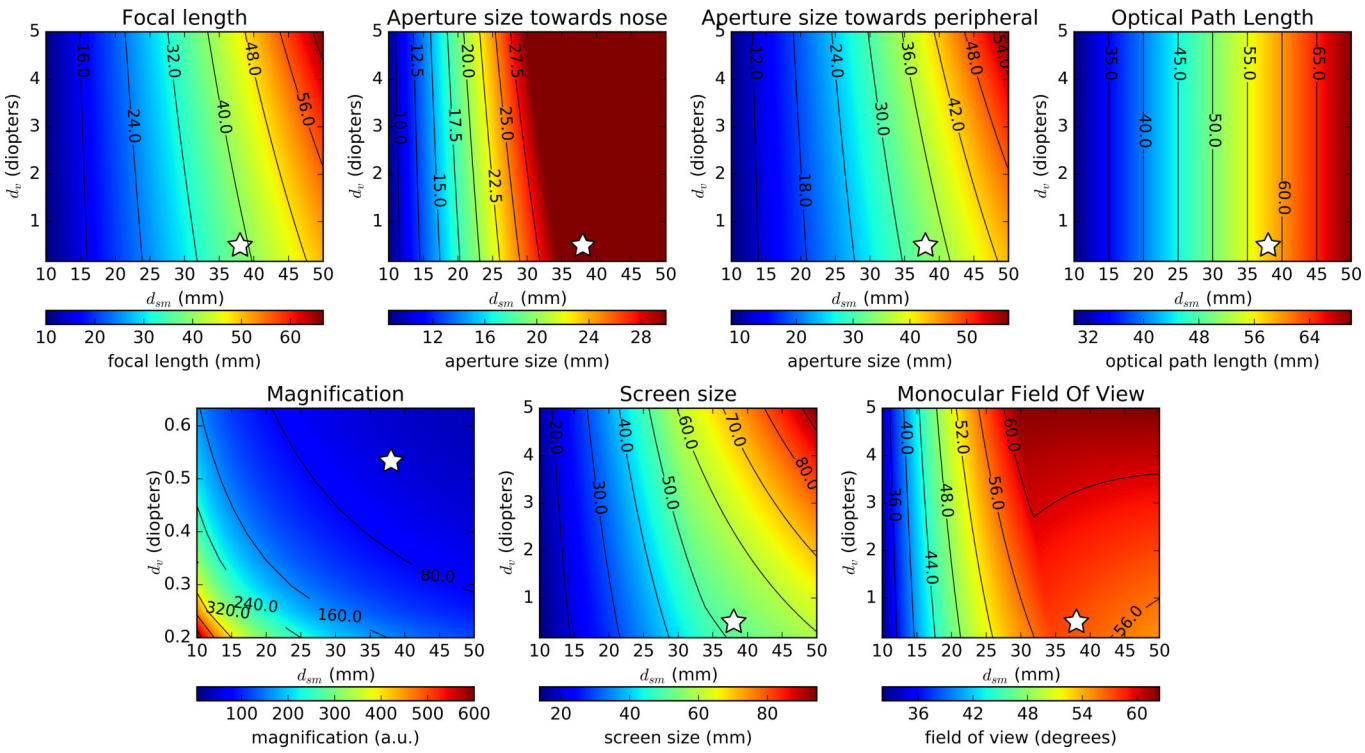

Fig. 4. One way to analyze the properties of our design is to graph the impact of two interacting free parameters on various dependent parameters. For a given virtual image plane at a distance d_v and an OASIIS screen to beam combiner distance d_{sm} configuration, from left to right, the first row of diagrams shows required focal length, beam combiner aperture size towards nose and peripheral vision, and optical path length. We indicate the prototype described in Section 4 with a star on each chart. Note that aperture size towards nose is naturally limited to half of interpupillary distance; we use 30 mm as the limit which would support most adults. Overall designs are limited with a f-number of $f/0.6$ to provide good imaging characteristics. For a given configuration, the second row of diagrams shows magnifications provided, required screen size, and horizontal monocular field of view provided.

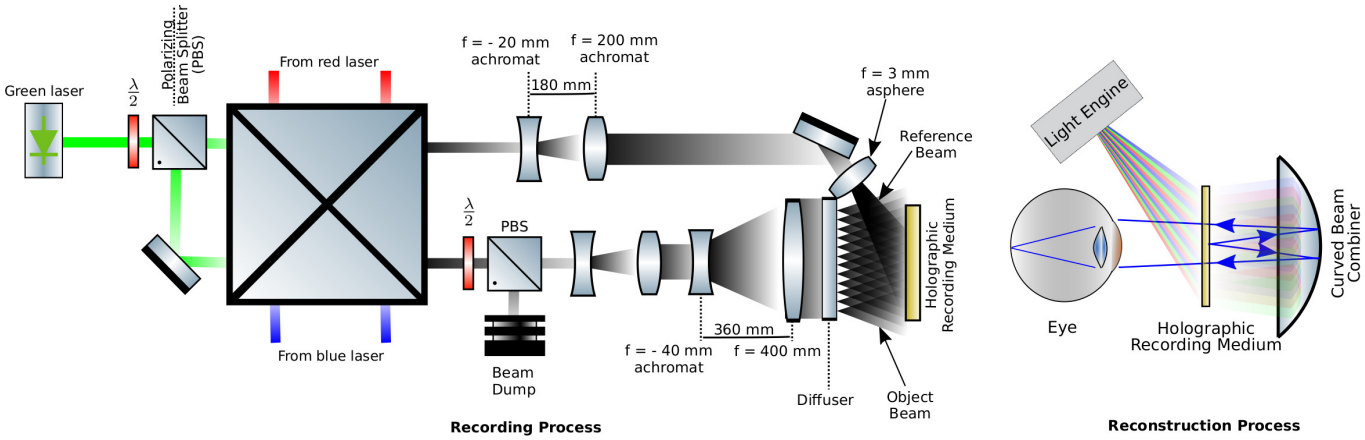

Fig. 5. Left: during recording, RGB light sources are combined to form a white light beam that is split into a reference beam and a object beam. A holographic recording medium captures the interference from both beams. Right: As a recorded medium is illuminated with lights from a light engine that closely resembles one of the original recording beams, the recorded medium diffuses light towards a curved beam combiner, which relays the resulting image on the recorded medium to the user's eye.

developed, re-exposing the diffraction pattern to the original reference beam (without the object beam present) recreates the object beam. The reconstructed object beam propagates in the same direction as the original object beam starting from the position of the

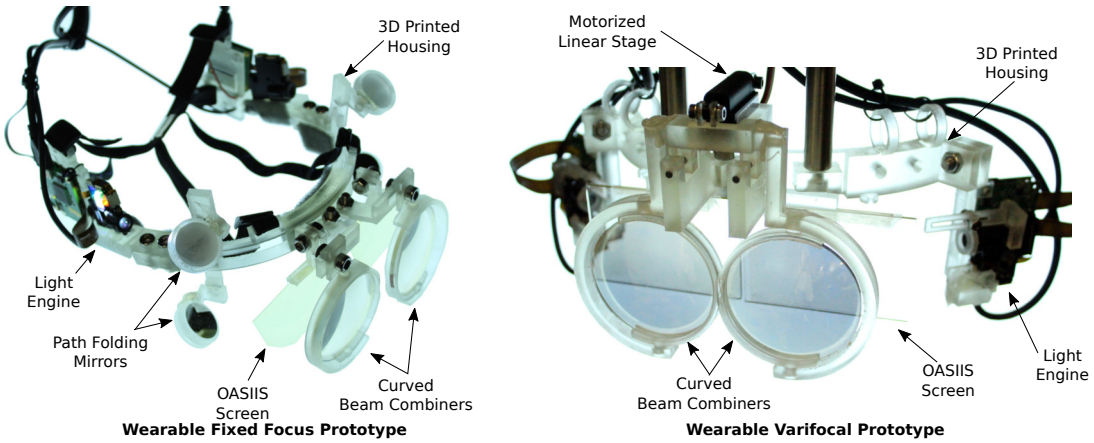

Fig. 6. Left: Our wearable fixed focus prototype using projection light engines, path-folding mirrors, curved beam combiners, 3D printed housing, and OASIIS screens. Right: Our wearable varifocal prototype using projection light engines, a motorized linear stage, curved beam combiners, 3D printed housing, and OASIIS screens.

hologram. The trick, for this project and others which create HOEs, is to come up with appropriate object and reference beams.

Figure 5 is a schematic diagram of the setup used in our experiments. We start with the recording process which is depicted in the left-hand part of the figure. The process starts on the left, where laser beams of three different colors (red, green, and blue) are split into two different beams with the help of a half-wave plate (labeled "$\frac{\lambda}{2}$") and a polarizing beam splitter (PBS). To simplify the diagram, only the green laser is depicted. These six beams are combined with an x-cube to form two different "white-light" beams (one horizontally polarized and the other vertically polarized). The horizontally polarized beam (top beam path) passes through a beam expander constructed from achromatic lenses with focal lengths −20 mm and 200 mm spaced by 180 mm which increases the diameter of the laser beam by a factor of 10. This beam is, then, reflected off of a mirror which directs the laser beam through a lens with a 3 mm focal length which forms the diverging reference beam for our experiment.

As shown in lower beam path in Figure 5, the object beam in the writing set-up is created by the vertically polarized beam. In order for the object and reference beams to interfere, the polarization of the object beam must be the same as the reference beam. The vertical polarization of the light in the lower beam path is rotated to horizontal with the help of another half-wave plate and a PBS. Excess light can be shunted off to a beam dump placed next to the PBS. Immediately following this, the diameter of the beam is increased by a factor of 100× with the help of two stages of beam expansion – one identical to the beam expansion used in the upper beam path and one made up of lenses with focal lengths of −40 mm and 400 mm. Upon passing through the last lens, the beam passes through a diffuser and forms the (diffusing) object beam.

The most demanding parts of the optical set-up are making sure that the original red, green, and blue laser beams are sufficiently collinear that they are well balanced at the position of the HRM and ensuring the beams leave each stage of beam expansion collimated. The requirements for the beams at the position of the HRM or the relative placement of the HRM from the last lens in the reference beam or from the diffuser are not precise. The distance of the HRM from the diffuser can be adjusted to change the relative intensity of the reference and object beams at the location of the HRM (but, this is more conveniently controlled with the half waveplate in the lower beam path). The only requirements for the final set of optics (the last lens in the reference beam path, the diffuser, and the HRM are that the beam intensities need to be loosely uniform and that the ratios of beam intensities need to be controlled (the ratio of reference to object beam intensities in our experiments were 1:10).

An additional requirements exist on the light sources used and the difference in the path length from the lasers to the HRM taken by light which travels either the top or the bottom beam path in Figure 5. The crests and troughs from the waves which make up the two beams must arrive at the location of the HRM with the same relative phase through out the recording process. In practice, this means that the light used in both beams need to come from the same laser source. The phase of a laser beam periodically resets in time to a new random value (temporal coherence). This limits the length over which a laser beam may be thought of as a single sinusoidal wave (the *coherence length*). Thus, to preserve the relative phase of the object and reference beams, the difference in path lengths that two beams travel must be less than the coherence length of the laser sources used. The recording process also depends on the wavelength. Care should also be taken to insure that the power density at each wavelength is similar in both beams at the location of the hologram. Exposure times should be chosen so as to achieve the desired total dosage at each wavelength (usually specified by the manufacturer in units of mJ/cm^2).

In our HMD design we construct the reference beam by placing the apparent origin of the "projection cone" of the projector at the same relative location to the HRM as location of the focus of the reference beam in the recording process. As mentioned before, when the hologram is illuminated with a beam which closely resembles the reference beam, this "reference beam" is diffracted by the hologram in such a way that it recreates the object beam. If the hologram is only partially illuminated by a part of the reference beam, then

only that part of the object beam which would originate from the illuminated part of the HOE is reconstructed. Also, if the hologram is illuminated with light which does not contain all of the wavelengths used to create the hologram, only those colors actually present in the reference beam will be present in the reconstructed object beam. Note that the difference between an "object beam" and a "reference beam" are arbitrary. Once the HOE is illuminated with light which closely resembles light from either beam, the part of the illuminated HOE will redirect light to create the corresponding part of the other beam, and all other beams will pass through the HOE as in Figure 1. The result is a thin, light-weight, see-through diffuser, which functions as an OASIIS screen.

3.3 Light Engine:

A projection-based light engine typically combines light-emitting diodes (LEDs) or lasers with modulation technologies such as liquid crystal on silicon (LCoS), digital micromirror device (DMD) or scanning microelectromechanical systems (MEMS). Scanning MEMS combined with laser sources promises an always-in-focus beam at different throw distances d_{throw}, whereas conventional LCoS coupled to lasers or LEDs require focusing optics. Having a large d_{throw} with LCoS or DMD modulators, however, more closely approximates an always-in-focus beam, and using LEDs decreases the amount of visible speckle phenomena largely. All of the mentioned light engines are applicable to our proposal as long as they are able to generate sharp pixels on our OASIIS screens at a given d_{throw}, thus current projectors are requiring a custom approach in projection optics, which we will discuss in up coming sections. Our design can act as a varifocal system by changing the distance between OASIIS screens and curved beam combiners, which can be achieved by either moving curved beam combiners or moving OASIIS screens. Moving curved beam combiners is practically less demanding from light engine requirements stand point, whereas in the other case projection has to be either always-in focus or has to provide adjustable focus to match a variable d_{throw}. Therefore, in our prototypes, we choose to move curved beam combiners and keep OASIIS screens at a fixed location.

4 IMPLEMENTATION

We provide the details for our prototypes, and explore the varifocal capabilities of our design. The OASIIS family of NED designs relies on a see-through screen co-axial with display and eye; we describe three example implementations using a mechanical rotating dot-pattern diffuser, PSDs, and HOEs as OASIIS screens.

4.1 Wearable Prototypes:

Our two wearable prototypes, one with fixed focus and one with varifocal capabilities, are shown in Figure 6. Modulated light from projection light engines is channeled through free space to OASIIS screens either directly or via path-folding mirrors, and information on OASIIS screens relayed to a user's eyes with partially reflective curved beam combiners.

Our light engines are commercially available pico-projectors that combine RGB LEDs to create a time-multiplexed white light source. Combined white light in our light engines is modulated using LCOS devices (OVP921, 1280×720 pixels, 60 Hz from ImagineOptix). Modulated light from our light engines approaches on OASIIS screens with a wide angle of 56^o, and forms a sharp image on OASIIS screens standing at $d_{\text{throw}} = 60 - 180$ mm in our two prototypes. In our fixed focus prototypes, we use silver coated off-the-shelf standard optical mirrors to fold the $d_{\text{throw}} = 180$ mm into a compact form factor. The OASIIS screens in our prototypes are interchangeable and can be PSDs (samples provided by Nitto Denko Corporation) or custom HOEs. In our varifocal prototype, location of a curved beam combiner is controlled by a Actuonix PQ12 linear actuator, and driven by an Arduino microcontroller (uC). Response time to shift of a beam combiner from one extreme to an another ($0.2 - 5$ D) is measured as 410 ms. A key question is whether a change in gaze can be determined and the focal adjustment accomplished, without hurting the ability to accommodate in practice. The control of accommodation is still under active investigation by vision scientists, and the driving mechanism probably rely on several input stimuli including chromatic characteristics [Kruger et al. 1995] and optical or computational blur [Ciuffreda et al. 2006; Del Águila-Carrasco et al. 2017]. There is also some reason to believe that varifocal systems can help driving accommodation as the total latency for accommodation is approximately one second [Campbell and Westheimer 1960]. There is some empirical evidence that varifocal systems similar to ours provide practical accomodation support in VR/AR contexts [Padmanaban et al. 2017] .

We use custom spherical concave mirrors (Diverse Optics) made from Zeonex. The inner mirror surface is coated with silver (beamsplitter coating 80% reflective, 20% transmissive). Our spherical mirrors have 76 mm radius of curvature and aperture size d_{aperture}, of 60 mm. In our prototypes, $d_e = 20$ mm and $d_{sm} = 37$ mm ($OPL = 57$ mm). All components of our prototypes are assembled with a 3D-printed housing built using a Formlabs 2 3D printer and FreeCAD software. We drive a prototype via two HDMI ports from a NVIDIA GeForce GTX 1080 on a Linux computer. The computer provides real-time imagery of 3D models using in-house built Python and OpenGL/GL Shader Languages based software while also compensating for mirror and keystone distortions.

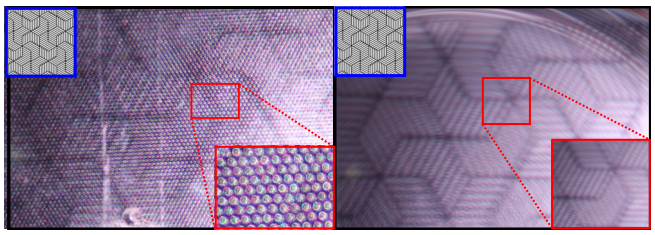

Fig. 7. Left: photograph showing a close look on the surface of a static dot-pattern diffuser illuminated with a projection light engine. Right: image formation when static dot-pattern diffuser is rotated around an axis with a conventional electrical motor.

4.2 Time-Multiplexed Dot-pattern Diffusers:

Our initial investigations used a simple and low-cost OASIIS screen: a dot-pattern projection surface, such as typically found in an LCD

backlight system [Chang and Fang 2007]. Dot-pattern screens contain a spatial pattern that is partially reflective and partially transmissive. We harvested a dot-pattern diffuser from a conventional LCD and rotated it rapidly with a small electrical motor to scan the entire area, providing a complete image when observed directly as demonstrated in Figure 7. Readers wishing to test OASIIS designs without producing HOEs will find this as a viable path when bulk and light loss are not major concerns. The significant backward scattering component will create undesired images on the screen–but much closer than the user's eye can focus, creating in effect a haze that reduces contrast but leaves the in-focus images easily perceivable.

4.3 Polarization Selective Diffusers:

PSDs scatter light that is linearly polarized in one direction (dictated during manufacture), but pass light that is polarized in the orthogonal direction. Extensive evaluation of the optical properties of PSDs can be found in [Seo and Kim 2008]. In our system we cause the PSD to diffuse the light from the light engine by placing a polarizer immediately after the light engine. A quarter waveplate applied on top of the PSD rotates the plane of polarization of the light so that, when passing back through the PSD, the reflected light is not diffused again. An anti-reflection coating applied to both surfaces of the PSD reduces reflections from the environment. Unfortunately, adding extra layers to a PSD comes with a trade-off: the multi-layered structure causes additional scattering. We measured the ratio of haze-generating component $I_{sb_0} + I_{sf_1}$ (see Figure 3) and image-forming component I_m (also Figure 3) in our PSD samples to be 8% when no coating is used and to be 14% with coatings. PSDs typically require linearly polarized light from a light engine, whereas in other approaches this is not the case.

4.4 Holography Setup:

Our best results for OASIIS screens come from our HOEs. We provide, here, the details of our holographic setup. A "white light" laser beam is created by combining the light from a Coherent Genesis MX460-500 SLM OPS Laser-Diode System, a Cobolt Samba diode pumped solid state laser and a Cobolt Flamenco diode pumped solid state laser operating at wavelengths of $532 - 460 - 660$ nm respectively. All three lasers have coherence lengths greater than 15 m. The holographic film used to record the HOEs was C-RT20 "Instant Hologram" Film (Litiholo). The beams were power balanced by placing a half waveplate and a polarizing beam splitter in front of each of the green and red lasers before combining the laser beams. Excess power was shunted into beam dumps. Beam expansion in Figure 5 was achieved using a Keplerian beam expander built with conventional achromatic lenses from Thorlabs. The diffuser used during the hologram writing process was a 250×250 mm 120 Grit Ground Glass Diffuser from Edmund Optics. Exposure times were controlled by a mechanical shutter (SH1/M, Thorlabs). Following exposure to the object and reference beams, "development" of the holographic pattern was finalized by exposing the holographic films to UV light (Dymax 2000-EC UV Light-Curing Flood Lamp) for 5 minutes. Once a holographic film is processed, it does not have to go through the same long process, and it can now act as an OASIIS screen. Note that a OASIIS screen is made to display dynamically changing imagery.

5 EXPERIMENTAL ASSESSMENT

Here we evaluate our experimental prototypes to assess optical qualities including FoV, eyebox, brightness, and varifocal range. We provide our examples in the supplementary video.

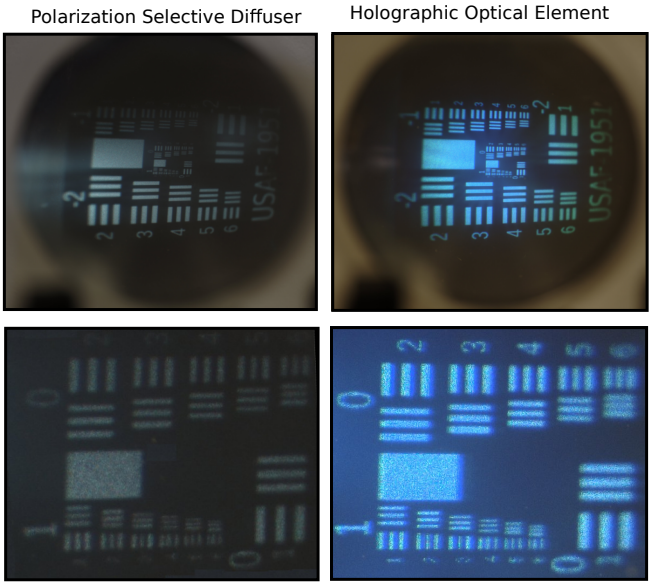

Fig. 8. A pair of photographs showing image quality and visible amount of haze while using (top left) a polarization selective diffuser with anti-reflection coating, and (top right) a holographic diffuser. Bottom row shows magnified central regions of top row.

Cakmakci and Rolland [2006] define wide FoV for NED designs as the ability to generate $> 60^o$ of monocular FoV. Depending on the user's facial structure, our prototypes provide a rotationally symmetric monocular FoV of $55^o - 63^o$. Many standards exist for reporting binocular FoV, including starting from a specific point inside a person's head (e.g., [Wearality 2015]) or starting from a "cyclopean eye" between the user's eyes (e.g., [Woods et al. 1993]). Especially in the case of varifocal NEDs, the differing approaches lead to widely varying estimates of the binocular FoV, and so we report only the well-understood measure of monocular FoV.

Our two OASIIS screen types, PSDs and HOEs provide different imaging characteristics as shown in Figure 8, in which brightness levels supported by each screen and point spread functions (PSFs) at various eccentricities are shown. We found HOEs to be more effective in our use cases. Note that phenomena of speckle is an artifact that can be observed for both types of OASIIS screens as can be seen in magnified regions in Figure 8, which can be mitigated through a dedicated light engine using moving diffusers in illumination mechanisms, broad-band illumination sources, or variation of polarization of light [Shevlin 2012]. Phenomena of speckle is more pronounced in HOEs, and this problem is traditionally tackled during recording process using moving diffusers [Gerritsen et al. 1968]

or using diffraction gratings [Utsugi and Yamaguchi 2013] during cloning the already recorded HOE. Following process of [Yang et al. 2012] in recording, An HOE can also be tuned for best color. We highlight that these are desired upgrades for our future work.

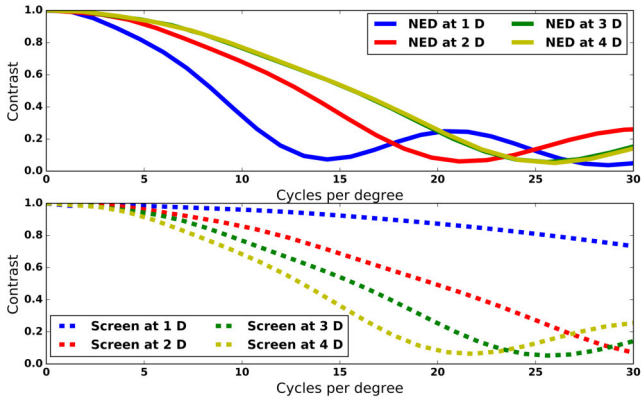

Fig. 9. A plot showing average Modulation Transfer Function (MTF) of near eye display's optical system at central field of view, while using a holographic optical element as an OASIIS screen. Our measurements are based on Slanted-Edge MTF methodology. We place a conventional desktop (27-inch Acer XB270HU) display at each depth level, and measure MTF of the display simultaneously using the same methodology to provide a comparison and a validation.

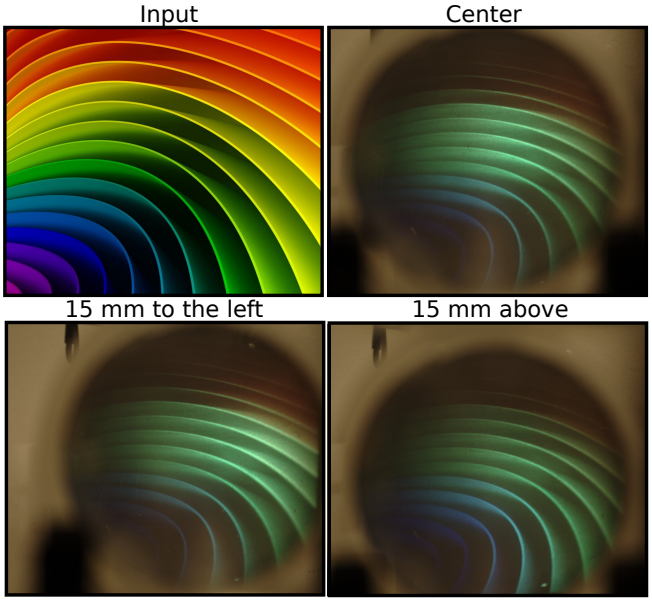

Fig. 10. Examination of eyebox stability. Top left: an input image provided to our light engine. Top right: A photograph taken from the center of our prototype's eyebox. Bottom left: A photograph taken from 15 mm to the left with respect to center of our prototype's eyebox. Bottom right: A photograph taken from 15 mm above the center of our prototype's eyebox.

We rely on off-the-shelf components so the keystone behavior comes from both the light engine and the angle that the light engine's projection axis makes with the normal vector of the HOE. The variation in PSFs across the FoV is primarily due to the projection geometry in our prototypes. The lenses in front of the light engine focus the light at a particular plane perpendicular to the light engine's projection axis. Since this plane is not parallel to the plane of the OASIIS screen, the effective size of the PSF changes across the FoV as the distance of the smallest spot size to the plane of the HOE changes. As in Figure 9, we also provide a detailed analysis of Modulation Transfer Functions (MTFs) of our prototype using HOEs at different depth levels. Our MTF measurements are based on a commonly accepted industry standard: ISO 122333 slanted-edge MTF method [Burns 2000]. The bottom part of Figure 9 provides MTF analysis of a conventional desktop display placed at highlighted depth ranges, and this data is included as a validation point of our analysis. The top part of Figure 9 shows the results of the same analysis on our device. A camera is placed behind our NED to mimic an eye position, and the camera is focused to a depth level, where a conventional display stands. A slanted edge is displayed on the conventional display at the position of central field of our NED, and thus generating data for the bottom portion of the figure as seen through our NED. Process is repeated by showing a slanted edge on our NED, and during experiments, NED's focus is always matched the camera's focus, which is at the conventional display in all experiments. Thus, we generated data for the top portion of the figure. Once the raw data is collected, a Gaussian blur is applied with a small enough kernel to decrease the noise in the image. We chose a region of interest at the FoV. We intentionally threshold the line spread function at 10% and 90% of intensities to avoid ripples in next step. Raw data is processed using the process in [Burns 2000], which can be briefly summarized as taking a Fast Fourier Transform (FFT) of a line spread function's first derivative. Note that as the conventional display gets closer to the camera, the angular extend of a single pixel on the conventional display increases and MTF falls from > 30 cpd to 12 cpd as expected. Our measurements indicate that, with our NED prototypes, achieving $18 - 20$ cpd is possible at the central regions of our FoV. However, as there isn't an available off-the-shelf light engine equipped for the task, at most extreme eccentricities resolutions drops to the level of 5 cpd. We observed high resolutions at different eccentricities, when our projection optics tuned to be at sharp focus at those eccentricities. Thus, we would like to highlight that resolution capabilities of our proposal are not limited with the demonstrated prototype and highly depending on the nature of a future projection optics. We will discuss further on overcoming this limitation in our future work section. Contradicting with the work of Konrad et al. [2017], our MTF measurements in Figure 9 suggest that supported resolution in cycles per degree drops with increasing virtual image distance. The major factor for this trend is due to large distance in between cornea and a spherical beam combiner in our system, $d_e + d_{sm} \approx 57$ mm, whereas this value is as small as 20 mm for [Konrad et al. 2017]. Effect of this distance on expected MTF is explained in detail in our supplementary.

We demonstrate the stability of our prototype's eyebox in Figure 10, which approximates a similar size as a consumer level conventional NED for VR. The light engines of our near eye display

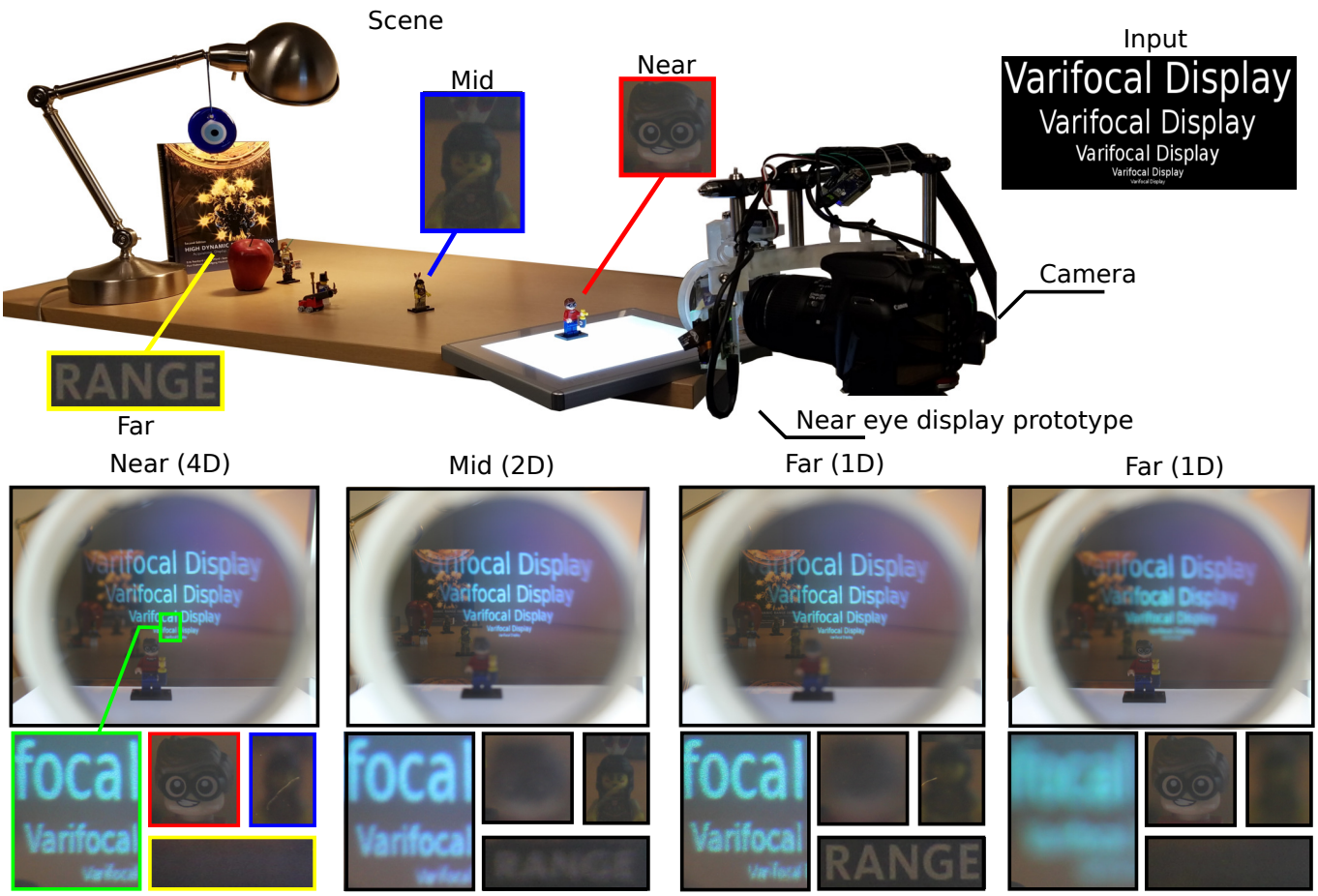

Fig. 11. Examination of varifocal performance using our holographic OASIIS screens. Top: shows the input image of our prototype and a real world scene with a near, a mid and a far target. As our curved beam combiner positioned by a linear motorized stage; the input image projected as the AR element. Middle shows four columns of data with the complete monocular FoV while AR element is projected at the highlighted depth levels. On the bottom in each column, insets show magnified images of the details of the targets at different depth levels and details of the AR element, which helps to interpret camera's focus for a given photograph.

prototype can provide up to 100 lumens while drive circuitries can also be programmed to set the brightness levels to a lower value. By projecting a wire-frame teapot model with 100 lumens, we evaluate the brightness performance of our prototypes in outdoor environment as in Figure 1, and we show that it can run even under strong sunlight.

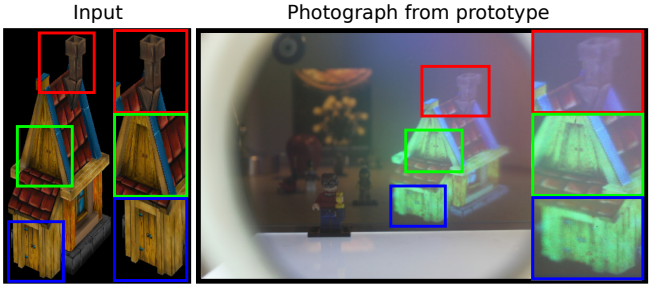

Fig. 12. Left: A rendered object provided as an AR element to our wearable varifocal prototype, Right: A photograph showing how our input AR element as seen through our wearable varifocal prototype.

In Figure 11, we demonstrate varifocal abilities of our design at indoors with a brightness level of 20 lumens using HOEs. To test for the feasibility, we translated the curved beam combiner back and forth up to $d_d = 5$ mm (see Figure 2) to cover a depth range of $1 - 4$ diopters. Using the same setup, as in Figure 12, we also provide a sample photograph providing information on the quality of a colored content.

Our display does not support occlusion of the real world by virtual objects. However, the brightness available to our design does make it viable the relative contrast mitigation strategy suggested by Rolland and Fuchs [2000], even when the real world is bright.

An early experimentations with our display and gaze tracking cameras from Pupil labs indicate that there are important items to

consider for an efficient gaze tracking integration; positioning and aiming of the camera with respect to eyebox has vital importance. Also accuracy, latency, and robustness of gaze tracking methodology plays an important role in defining operations or applications for our prototypes. Expected idle location for placing cameras is directly in front of the eye, however as this isn't directly feasible for our prototype without inserting a beam splitter, we placed cameras below HOEs and this limits the quality of the capture for tracking. The gaze tracking cameras that works under strong sunlight or outdoors is also an important item that has to be tackled, this is known to be a general problem for gaze tracker designers as bright ambients can easily saturate cameras. All these open questions leave challenges to gaze tracker manufacturers and researchers in the next step of AR devices.

6 LIMITATIONS AND FUTURE WORK

While this design opens up new research opportunities, work remains to overcome practical challenges to producing a commercially viable product. For both HOEs and PSDs, we observe slightly different brightness levels across the visual field as can be observed in Figure 8. We can improve the HOE's response to be more homogeneously distributed by improving the beam shaping optics of our object beam.

Recording a HOE with a reference beam going through a replica of targeted light engine optics would help resolve color issues across all visual fields, as it truly mimics light engines behavior. Instead of off-axis projection, using waveguides as done by Travis et al. [2013] could also result in separate-waveguide systems at different distances to the eye, bringing the work of Lee et al. [2016] to a NED use case. Of course, light levels emitted by the light engine can also be adjusted in image space to even out perceived light levels. Finally, using a microlens array HOE [Yeom et al. 2014] as an OASIIS screen, combined with the near-eye lightfield display of Lanman and Luebke [2013], could extend our approach to AR lightfields.

Using a thicker holographic recording medium than used in this study would increase light efficiency and allow the light engines to use less power. This improvement comes with a design trade-off. Thin holographic diffusers have a wide spectral response [Gu et al. 1996] which allows us to use our HOE diffusers with conventional light engines, whereas thick HOEs provide a narrow wavelength response and would require careful tuning of HOE to light engine wavelength.

Image degradations across our display's visual field and keystone effect are both caused by off-axis projection, both items can be corrected through a custom light engine design [Maimone et al. 2017] or possibly by a focus sweeping projection or display optics design [Iwai et al. 2015; Konrad et al. 2017]. Linear actuators used in our system can also be replaced with the design of Dunn et al. [2017] as the form factor of the deformable mirror membranes shrink in size in the near future.

While our prototype is not large by the standards of wide FoV NED systems, with the form factor of ski goggles, it is still bulky compared to corrective glasses. The design space shown in Figure 4 suggests some avenues for miniaturization. Work of Ren et al. [2016] observed a significant increase in task based performance with increasing FoV, thus hinting for a need of even large FoV. We speculate that recording curved OASIIS screens similar to Guillaumee et al. [2014] and using a more complex surface model for the combiner may improve FoV. In the supplement to this paper we provide code to generate design candidates for a free-form combiner that exceeds 80^o. In a commercial product, varying ambient light levels could be detected with a photo-detector and appropriate light levels could be displayed by a continuously varying neutral density filter (i.e., Thorlabs NDC-25C-2) or by adjusting the emissive power of the light engine. Such additions may lead naturally to High Dynamic Range [Lincoln et al. 2017; Seetzen et al. 2004] NED systems.

7 CONCLUSION

We have presented a novel family of designs for see-through near-eye display devices. Our approach, dubbed OASIIS, uses an on-axis see-through screen to form an intermediate image which is then relayed back toward the eye by a concave mirror or a partially-transparent beam combiner. The resulting system is simple to design and construct, with robust and inexpensive components. The OASIIS design advances several goals of augmented reality, including wide field of view, large eyebox, unobstructed peripheral view beyond the display, high image quality, no chromatic aberration, and real-world imagery undistorted by refractive or diffractive elements. Our wearable prototypes resemble current virtual reality devices in size, but we believe the design lends itself to a compact miniaturized wearable device. Finally, slight deflections of the lightweight curved beam combiners enable the display to rapidly change focal plane, opening an intriguing avenue for future work on accommodation-supporting augmented reality display.

ACKNOWLEDGEMENTS

The authors would like to thank reviewers for their valuable feedback. We also thank Josef Spjut for fruitful discussions and for his guidance on linear actuators and Ikuo Kawamoto of Nitto Japan for providing samples of the polarization selective scatterers.

REFERENCES

Gerhard Ackermann and Juergen Eichler. 2007. *Holography: A Practical Approach*. Wiley-VCH Verlag GmbH & Co. KGaA, Weinheim.

Kurt Akeley, Simon J Watt, Ahna Reza Girshick, and Martin S Banks. 2004. A stereo display prototype with multiple focal distances. In *ACM transactions on graphics (TOG)*, Vol. 23. ACM, 804–813.

Peter D Burns. 2000. Slanted-edge MTF for digital camera and scanner analysis. In *Is and Ts Pics Conference*. SOCIETY FOR IMAGING SCIENCE & TECHNOLOGY, 135–138.

Ozan Cakmakci and Jannick Rolland. 2006. Head-worn displays: a review. *Journal of Display Technology* 2, 3 (2006).

FW Campbell and G Westheimer. 1960. Dynamics of accommodation responses of the human eye. *The Journal of Physiology* 151, 2 (1960), 285–295.

Jee-Gong Chang and Yu-Bin Fang. 2007. Dot-pattern design of a light guide in an edge-lit backlight using a regional partition approach. *Optical Engineering* 46, 4 (2007).

Dewen Cheng, Yongtian Wang, Hong Hua, and MM Talha. 2009. Design of an optical see-through head-mounted display with a low f-number and large field of view using a freeform prism. *Applied Optics* 48, 14 (2009).

Kenneth J Ciuffreda, Arkady Selenow, Bin Wang, Balamurali Vasudevan, George Zikos, and Steven R Ali. 2006. Bothersome blur: A functional unit of blur perception. *Vision research* 46, 6 (2006), 895–901.

Antonio J Del Águila-Carrasco, Iván Marín-Franch, Paula Bernal-Molina, José J Esteve-Taboada, Philip B Kruger, Robert Montés-Micó, and Norberto López-Gil. 2017. Accommodation Responds to Optical Vergence and Not Defocus Blur AloneAccommodation Responds to Optical Vergence. *Investigative Ophthalmology & Visual Science* 58, 3 (2017), 1758–1763.

Justin G Droessler and Donald J Rotier. 1990. Tilted cat helmet-mounted display. *Optical Engineering* 29, 8 (1990).

D. Dunn, C. Tippets, K. Torell, P. Kellnhofer, K. Akşit, P. Didyk, K. Myszkowski, D. Luebke, and H. Fuchs. 2017. Wide Field Of View Varifocal Near-Eye Display Using See-Through Deformable Membrane Mirrors. *IEEE Transactions on Visualization and Computer Graphics* (2017).

Leon Eisen, Michael Meyklyar, Michael Golub, Asher A. Friesem, Ioseph Gurwich, and Victor Weiss. 2006. Planar conĭnĝuration for image projection. *Applied Optics* 45, 17 (2006).

HJ Gerritsen, WJ Hannan, and EG Ramberg. 1968. Elimination of speckle noise in holograms with redundancy. *Applied optics* 7, 11 (1968), 2301–2311.

Pinhas Gilboa. 1991. Designing the right visor. In *Medical Imaging*. International Society for Optics and Photonics.

Patrick Görrn, Michelle Sander, Jens Meyer, Michael Kröger, Eike Becker, H-H Johannes, Wolfgang Kowalsky, and Thomas Riedl. 2006. Towards see-through displays: fully transparent thin-film transistors driving transparent organic light-emitting diodes. *Advanced Materials* 18, 6 (2006).

Claire Gu, Jenn-Ren Lien, Foster Dai, and John Hong. 1996. Diffraction Properties of Volume Holographic Diffusers. *Journal of the Optical Society of America A, Optics and Image Science* 13, 8 (08 1996).

Mickael Guillaumee, Seyed Payam Vahdati, Eric Tremblay, Arnaud Mader, Gabriel Bernasconi, Victor J. Cadarso, Jonas Grossenbacher, Juergen Brugger, Randall Sprague, and Christophe Moser. 2014. Curved Holographic Combiner for Color Head Worn Display. *Journal of Display Technology* 10, 6 (2014).

M Kivanc Hedili, Mark O Freeman, and Hakan Urey. 2013. Microlens array-based high-gain screen design for direct projection head-up displays. *Applied Optics* 52, 6 (2013).

Chia Wei Hsu, Bo Zhen, Wenjun Qiu, Ofer Shapira, Brendan G DeLacy, John D Joannopoulos, and Marin Soljačić. 2014. Transparent displays enabled by resonant nanoparticle scattering. *Nature Communications* 5 (2014).

Xinda Hu and Hong Hua. 2014. High-resolution optical see-through multi-focal-plane head-mounted display using freeform optics. *Optics express* 22, 11 (2014).

Hong Hua. 2017. Enabling Focus Cues in Head-Mounted Displays. *Proc. IEEE* 105, 5 (2017), 805–824.

Hong Hua and Bahram Javidi. 2014. A 3D integral imaging optical see-through head-mounted display. *Optics express* 22, 11 (2014).

Fu-Chung Huang, Kevin Chen, and Gordon Wetzstein. 2015. The light field stereoscope: immersive computer graphics via factored near-eye light field displays with focus cues. *ACM Transactions on Graphics (TOG)* 34, 4 (2015).

Daisuke Iwai, Shoichiro Mihara, and Kosuke Sato. 2015. Extended depth-of-field projector by fast focal sweep projection. *IEEE Transactions on Visualization and Computer Graphics* 21, 4 (2015), 462–470.

Paul V Johnson, Jared AQ Parnell, Joohwan Kim, Christopher D Saunter, Gordon D Love, and Martin S Banks. 2016. Dynamic lens and monovision 3D displays to improve viewer comfort. *Optics Express* 24, 11 (2016).

Hee-jae Kim, Sung-Keun Lee, Mei-Lan Piao, Nam Kim, and Jae-Hyeung Park. 2015. Three-dimensional holographic head mounted display using holographic optical element. In *Consumer Electronics (ICCE), 2015 IEEE International Conference on*. IEEE, 132–133.

Robert Konrad, Emily A Cooper, and Gordon Wetzstein. 2016. Novel optical configurations for virtual reality: evaluating user preference and performance with focus-tunable and monovision near-eye displays. In *Human Factors in Computing Systems*.

Robert Konrad, Nitish Padmanaban, Keenan Molner, Emily A Cooper, and Gordon Wetzstein. 2017. Accommodation-invariant computational near-eye displays. *ACM Transactions on Graphics (TOG)* 36, 4 (2017), 88.

Gregory Kramida and Varshney Amitabh. 2016. Resolving the Vergence-Accommodation Conflict in Head-Mounted Displays. *IEEE Transactions on Visualization and Computer Graphics* 22, 7 (2016).

Bernard Kress and Meimei Shin. 2013. Diffractive and holographic optics as optical combiners in head mounted displays. In *Pervasive and Ubiquitous Computing Adjunct Publication*.

Bernard Kress and Thad Starner. 2013. A review of head-mounted displays (HMD) technologies and applications for consumer electronics. In *SPIE Defense, Security, and Sensing*. International Society for Optics and Photonics.

Philip B Kruger, Sujata Nowbotsing, Karan R Aggarwala, and Steven Mathews. 1995. Small amounts of chromatic aberration influence dynamic accommodation. *Optometry & Vision Science* 72, 9 (1995), 656–666.

Douglas Lanman and David Luebke. 2013. Near-eye light field displays. *ACM Transactions on Graphics (TOG)* 32, 6 (2013).

Seungjae Lee, Changwon Jang, Seokil Moon, Jaebum Cho, and Byoungho Lee. 2016. Additive light field displays: realization of augmented reality with holographic optical elements. *ACM Transactions on Graphics (TOG)* 35, 4 (2016).

Gang Li, Dukho Lee, Youngmo Jeong, Jaebum Cho, and Byoungho Lee. 2016. Holographic display for see-through augmented reality using mirror-lens holographic optical element. *Optics letters* 41, 11 (2016).

Peter Lincoln, Alex Blate, Montek Singh, Andrei State, Mary C. Whitton, Turner Whitted, and Henry Fuchs. 2017. Scene-adaptive high dynamic range display for low latency augmented reality. In *Proceedings of the 21st ACM SIGGRAPH Symposium on Interactive 3D Graphics and Games*. ACM, 15.

Gabriel Lippmann. 1908. Epreuves reversibles. photographies integrals. *Comptes-Rendus Academie des Sciences* 146 (1908).

Sheng Liu, Dewen Cheng, and Hong Hua. 2008. An optical see-through head mounted display with addressable focal planes. In *International Symposium on Mixed and Augmented Reality*.

Chenguang Ma, Jinli Suo, Qionghai Dai, Ramesh Raskar, and Gordon Wetzstein. 2013. High-rank coded aperture projection for extended depth of field. In *Computational Photography (ICCP)*. IEEE.

Kevin J MacKenzie, David M Hoffman, and Simon J Watt. 2010. Accommodation to multiple-focal-plane displays: Implications for improving stereoscopic displays and for accommodation control. *Journal of vision* 10, 8 (2010), 22–22.

Andrew Maimone, Andreas Georgiou, and Joel Kollin. 2017. Holographic Near-Eye Displays for Virtual and Augmented Reality. *ACM Transactions on Graphics* 36 (2017).

Andrew Maimone, Douglas Lanman, Kishore Rathinavel, Kurtis Keller, David Luebke, and Henry Fuchs. 2014. Pinlight Displays: Wide Field of View Augmented Reality Eyeglasses Using Defocused Point Light Sources. *ACM Trans. Graph.* 33, 4 (2014).

Belen Masia, Gordon Wetzstein, Piotr Didyk, and Diego Gutierrez. 2013. A survey on computational displays: Pushing the boundaries of optics, computation, and perception. *Computers & Graphics* 37, 8 (2013), 1012–1038.

Nathan Matsuda, Alexander Fix, and Douglas Lanman. 2017. Focal surface displays. *ACM Transactions on Graphics (TOG)* 36, 4 (2017), 86.

Nitish Padmanaban, Robert Konrad, Tal Stramer, Emily A Cooper, and Gordon Wetzstein. 2017. Optimizing virtual reality for all users through gaze-contingent and adaptive focus displays. *Proceedings of the National Academy of Sciences* (2017), 201617251.

Donghao Ren, Tibor Goldschwendt, YunSuk Chang, and Tobias Höllerer. 2016. Evaluating wide-field-of-view augmented reality with mixed reality simulation. In *Virtual Reality (VR), 2016 IEEE*. IEEE, 93–102.

Jannick P Rolland and Henry Fuchs. 2000. Optical versus video see-through head-mounted displays in medical visualization. *Presence: Teleoperators and Virtual Environments* 9, 3 (2000).

Donald J Rotier. 1989. Optical approaches to the helmet mounted display. In *1989 Orlando Symposium*. International Society for Optics and Photonics.

Graham Saxby and Stanislovas Zacharovas. 2016. *Practical Holography* (fourth edition ed.). CRC Press, Taylor & Francis Group, LLC, 6000 Broken Sound Parkway, NW, Suite 300, Boca Raton, FL 33487-2742.

Helge Seetzen, Wolfgang Heidrich, Wolfgang Stuerzlinger, Greg Ward, Lorne Whitehead, Matthew Trentacoste, Abhijeet Ghosh, and Andrejs Vorozcovs. 2004. High dynamic range display systems. *ACM Transactions on Graphics (TOG)* 23, 3 (2004).

Jong-Wook Seo and Taeho Kim. 2008. Double-layer projection display system using scattering polarizer film. *Japanese Journal of Applied Physics* 47, 3R (2008).

Fergal P Shevlin. 2012. Speckle reduction in laser-illuminated picoprojectors. In *Proc. SPIE*, Vol. 8252. 825206.

Takashi Shibata, Takashi Kawai, Keiji Ohta, Masaki Otsuki, Nobuyuki Miyake, Yoshihiro Yoshihara, and Tsuneto Iwasaki. 2005. Stereoscopic 3-D display with optical correction for the reduction of the discrepancy between accommodation and convergence. *Journal of the Society for Information Display* 13, 8 (2005), 665–671.

Shoaib R Soomro and Hakan Urey. 2016. Design, fabrication and characterization of transparent retro-reflective screen. *Optics Express* 24, 21 (2016).

T Sugihara and T Miyasato. 1998. A Lightweight 3-D HMD with Accommodative Compensation. In *SID Symposium Digest of Technical Papers*, Vol. 29. Wiley Online Library, 927–930.

Ivan E Sutherland. 1968. A head-mounted three dimensional display. In *Proceedings of the December 9-11, 1968, Fall Joint Computer Conference, part I*. ACM.

Elen Tolstik, Alexander Winkler, Vladislav Matusevich, Richard Kowarschik, Uladzimir V. Mahilny, Dzianis N. Marmysh, Yuri Ivanovich Matusevich, and Leonid Petrovich Krul. 2009. PMMA-PQ Photopolymers for Head-Up-Displays. *IEEE Photonics Technology Letters* 21, 12 (2009).

Adrian RL Travis, Timothy A Large, Neil Emerton, and Steven N Bathiche. 2013. Wedge optics in flat panel displays. *Proc. IEEE* 101, 1 (2013).

Yu-Hsiang Tsai, Mao-Hsiu Huang, Ting-Wei Huang, Kuo-Lung Lo, Mang Ou-Yang, et al. 2015. Image quality affected by diffraction of aperture structure arrangement in transparent active-matrix organic light-emitting diode displays. *Applied Optics* 54, 28 (2015).

Hakan Urey. 2000. Optical advantages in retinal scanning displays. In *AeroSense 2000*. International Society for Optics and Photonics.

Takeru Utsugi and Masahiro Yamaguchi. 2013. Reduction of the recorded speckle noise in holographic 3D printer. *Optics express* 21, 1 (2013), 662–674.

Junhua Wang, Yuechao Liang, and Min Xu. 2016. Design of a See-Through Head-Mounted Display with a Freeform Surface. *Journal of the Optical Society of Korea* 19, 6 (2016).

Technical Staff Wearality. 2015. *Wearality Sky Field of View.* White Paper. http://wearality.com/WearalitySkyFieldOfView.pdf

Paul Webb. 1964. Bioastronautics data book. (1964).

Andrew J Woods, Tom Docherty, and Rolf Koch. 1993. Image distortions in stereoscopic video systems. In *IS&T/SPIE's Symposium on Electronic Imaging: Science and Technology*. International Society for Optics and Photonics.

Akira Yamamoto, Yujiro Yanai, Michio Nagai, Ryo Suzuki, and Yoji Ito. 2016. 16-3: A Novel Transparent Screen Using Cholesteric Liquid Crystal Dots. *Digest of Technical Papers* 47, 1 (2016).

Fei Yang, Yuri Murakami, and Masahiro Yamaguchi. 2012. Digital color management in full-color holographic three-dimensional printer. *Applied optics* 51, 19 (2012), 4343–4352.

Jiwoon Yeom, Jinsoo Jeong, Changwon Jang, Keehoon Hong, Soon-gi Park, and Byoungho Lee. 2014. Reflection-type integral imaging system using a diffuser holographic optical element. *Optics express* 22, 24 (2014), 29617–29626.